High energy proton stripping by ^{27}Al and ^{28}Si nuclei: Ground state transitions

A. Djaloeis, S. Gopal, J. Bojowald, W. Oelert, N. G. Puttaswamy, and P. Turek
Institut für Kernphysik, Kernforschungsanlage Jülich, D-5170 Jülich, West Germany

C. Mayer-Böricke
Institut für Kernphysik, Kernforschungsanlage Jülich, D-5170 Jülich, West Germany and Department of Physics, University of Bonn, D-5300 Bonn, West Germany

(Received 12 April 1982)

Angular distributions for the ^{27}Al$(h,d_0)^{28}$Si and ^{28}Si$(h,d_0)^{29}$P reactions have been measured at $E_h=130$ MeV in the $9^\circ \lesssim \theta_{c.m.} \lesssim 40^\circ$ angular range. The data have been analyzed in terms of the distorted-wave Born approximation theory. Finite-range and nonlocality effects are found to be significant and are necessary for a good description of the experimental data. The extracted spectroscopic strengths are $G(2s_{1/2}) = 0.89 \pm 0.18$ and $G(1d_{5/2}) = 0.22 \pm 0.04$ for the ^{28}Si$(h,d_0)^{29}$P and ^{27}Al$(h,d_0)^{28}$Si reactions, respectively. The former value agrees well with that predicted by a shell-model calculation performed in a full $1d_{5/2}$-$2s_{1/2}$-$1d_{3/2}$ basis space; the latter, however, is only about 40% of the predicted value.

[NUCLEAR REACTIONS ^{27}Al, ^{28}Si(h,d_0), $E=130$ MeV; measured $\sigma(E,\theta)$. DWBA analysis, deduced spectroscopic strengths. Enriched targets.]

I. INTRODUCTION

In the shell model picture, stripping reactions provide a method of inserting nucleons into available orbits in a nucleus. For reactions involving a direct one-nucleon stripping, the cross section for transition to a specific orbit can be factorized into two parts, one related to the nuclear structure involved, the other describing the dynamics of the reaction. The latter is generally described in terms of the distorted wave Born approximation (DWBA) and is used to extract nuclear structure information (spectroscopic strength, see Sec. III) from the experimental data.

Although, in principle, the spectroscopic strength should be independent of the reaction type and incident energy, it is found[1] that the experimentally extracted quantities often do not show this feature. In addition, they are not only found to differ among themselves, but also often are different from those calculated on the basis of, e.g., the nuclear shell model[2] (see Sec. III C). For proton stripping by ^{27}Al and ^{28}Si, the presently available information is given in Sec. III C.

We have performed proton stripping experiments on ^{27}Al and ^{28}Si targets through the (h,d) reaction at $E_h=130$ MeV. In this paper, we report the experimental results and their analysis for the ground-state transitions which involve two different single (lj) transfers, namely $(d_{5/2})$ and $(s_{1/2})$ for the ^{27}Al$(h,d_0)^{28}$Si and ^{28}Si$(h,d_0)^{29}$P reactions, respectively. For these two experimental angular distributions, we have studied systematically the dynamical aspects of the reactions in order to obtain a consistent set of best-fit DWBA parameters. Using these parameters the spectroscopic information has been extracted and compared with that available in the literature (see Sec. III C). The DWBA parameters will also be used in the analysis of the transitions leading to the excited states in the residual nuclei. The results will be presented in a forthcoming paper.[3]

II. EXPERIMENT

The experiment was performed at the isochronous cylcotron JULIC. The extracted h beam ($\Delta E/E \sim 0.3\%$) hit the target without prior momentum analysis. Beam intensities ranging from a few nA at most forward angles up to ~ 200 nA at larger angles were used. The targets ^{27}Al and ^{28}Si were self-supporting foils, about 5 mg/cm^2 thick. The charged reaction products were detected by two

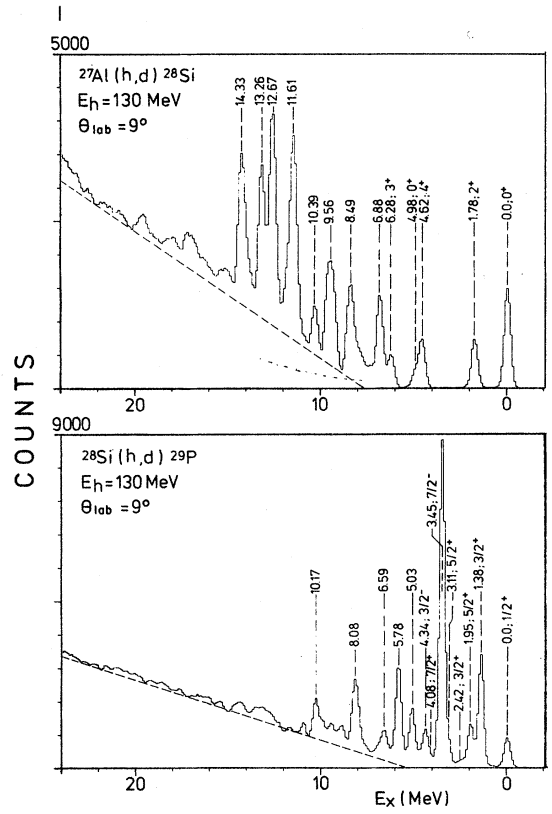

FIG. 1. Deuteron spectra from the ^{27}Al$(h,d)^{28}$Si and ^{28}Si$(h,d)^{29}$P reactions at $\theta_{lab}=9°$.

$\Delta E-E$ telescopes mounted 3° apart from each other inside a 1 m diameter scattering chamber. Side-entry 31 mm-thick Ge(Li) detectors[4] were used as E counters. A choice of 1 mm ΔE counters was made as a compromise between the particle detection cutoff at low energies and the good particle separation. Each telescope was coupled through standard electronics to two particle identifier units to achieve optimal separation for the p-d-t and for the h-α particle groups. A tantalum collimating system (with an angular opening $\Delta\theta\sim0.4°$), thick enough to stop high energy protons, was placed in front of each telescope. A Ge (Li) monitor detector was situated at a fixed angle of $\theta_L=-30°$. Energy calibration was accomplished using a CH_2-CD_2-Au target. Figure 1 shows the measured d spectra for ^{27}Al and ^{28}Si targets taken at $\theta_L=9°$. The overall energy resolution is about 500 keV. It can be seen that the peaks corresponding to the ground-state transitions are well separated. Peak identification follows from the energy calibration and the Endt and van der Leun compilation.[1] The angular distributions for the transition to the ground states of the ^{28}Si and ^{29}P residual nuclei have been extracted in the $9°\lesssim\theta_{c.m.}\lesssim40°$ angular range. The error bar associated with each of the experimental points (see, e.g., Fig. 3) represents the total error which includes both the relative and the absolute uncertainties. This total error varies from about $\pm10\%$ to $\pm30\%$ in the measured angular range.

III. ANALYSIS

The (h,d) reaction is assumed to proceed through a direct proton stripping. The theoretical cross section is calculated in the framework of the DWBA formalism. Effects of the finite-range are studied by exact (EFR) and approximate (AFR) methods employing the computer codes DWUCK5[5] and DWUCK4,[6] respectively. Effects of nonlocality (NL) corrections are studied using the DWUCK4 program only since DWUCK5 does not have this option. The relation between the experimental $(d\sigma/d\Omega)_{exp}$ and theoretical $(d\sigma/d\Omega)_{DW}$ cross section for a (h,d) reaction, in the two computer programs, is given by[5,6]

$$(d\sigma/d\Omega)_{exp}=N\sum_{lj}\frac{G(nlj)}{K_j}(d\sigma/d\Omega)_{DW},$$

where

$$G(nlj)=\frac{2J_f+1}{2J_i+1}C^2S(nlj),$$

$K_j=2j+1$ and $N=4.42$ for DWUCK4[6] and $K_j=1$ and $N=1$ for DWUCK5.[5] The quantity C^2 is the isospin coupling coefficient, $S(nlj)$ is the spectroscopic factor, and $G(nlj)$ is the spectroscopic strength for the proton stripped into the orbit specified by the principal quantum number n and by the orbital and total angular momentum l and j, respectively. The initial (target) and the final (residual nucleus) spins are denoted by J_i and J_f, respectively.

The value of $G(nlj)$ is extracted by matching the theoretical angular distribution to the experimental one. In the present work the error associated with $G(nlj)$ is estimated to be about $\pm20\%$, which reflects the error on the data as well as the uncertainty in the curve matching procedure.

A. Input parameters

A list of the optical model potential (OMP) and DWBA parameters used in the present work is given in Table I. The radial wave function of the

TABLE I. Optical-model and DWBA parameters. In all sets $r_c = 1.3$ fm. Proton bound-state parameter: $\lambda = 25.0$ (Thomas spin-orbit form), $r_0 = 1.25$ fm, and $a = 0.65$ fm. Nonlocality parameter: $\beta(p) = 0.85$ fm^{-1}, $\beta(h) = 0.25$ fm^{-1}, $\beta(d) = 0.54$ fm^{-1}, see Ref. 8. Finite-range parameter: $R = 0.77$ fm.

	Set	V^c (MeV)	r_v (fm)	a_v (fm)	W_s^d (MeV)	W_v^c (MeV)	r_w (fm)	a_w (fm)	V_{so} (MeV)	r_{so} (fm)	a_{so} (fm)	Reference
h^a:	JVSH	111.0	1.128	0.856		21.6	1.613	0.643				Present
	JSSH	110.0	1.113	0.860	20.2		1.105	0.833				Present
	DVSH	110.0	1.084	0.973		28.4	1.466	0.707				Present
	DSSH	110.0	1.081	0.988	19.9		1.050	0.886				Present
d^b:	DMSD1	55.0	1.170	0.873	3.0	13.1	1.262	0.730	3.0	1.070	0.660	9
	DMSD2	55.0	1.170	0.873	3.0	13.1	1.262	0.730	6.0	1.070	0.660	Present
	BSSD1	47.0	1.180	0.720	10.0		1.15	0.900	12.5	1.100	1.000	10
	BSSD2	47.0	1.180	0.720	10.0		1.150	0.900	6.0	1.100	1.000	Present
	BSSD3	47.0	1.180	0.720	10.0		1.150	0.900	6.0	1.180	0.720	Present
	BMSD4	58.9	1.180	0.754	5.5	7.6	1.270	0.814	6.0	0.900	0.900	11

[a]The analytical form of the potential shapes is given in Ref. 7.
[b]The analytical form of the potential shapes is given in Ref. 9.
[c]Woods-Saxon.
[d]Woods-Saxon derivative.

proton stripped by the ^{27}Al and ^{28}Si targets was generated in a real Woods-Saxon (WS) potential with a Thomas spin-orbit term and including a Coulomb term corresponding to a uniform spherical charge. The WS-potential depth was automatically varied in the computer program until the correct binding energy was reproduced.

No experimental data and the corresponding optical model analysis of deuteron elastic scattering at incident energies $E_d \geq 90$ MeV are available so far for the reactions studied in this work. Therefore, for sets DMSD1 and BSSD1 (see Table I), the parameter values of the deuteron potential in the exit channel were determined from the target mass and incident energy dependence of the deuteron potential reported by Daehnick *et al.*[9] and Bojowald *et al.*,[10] respectively. For both sets, the depth V of the real part was found to be about 50 MeV. One should note that the extrapolated V_{so} values seem to be too weak and too strong for the DMSD1 and BSSD1, respectively, compared to $V_{so} \sim 6$ MeV predicted by the folding model[11]; this value (~ 6 MeV) has generally been used in the analyses of deuteron elastic scattering angular distribution and polarization data at lower incident energies.[9] Furthermore, in set BSSD1, the value of a_{so} is sig-

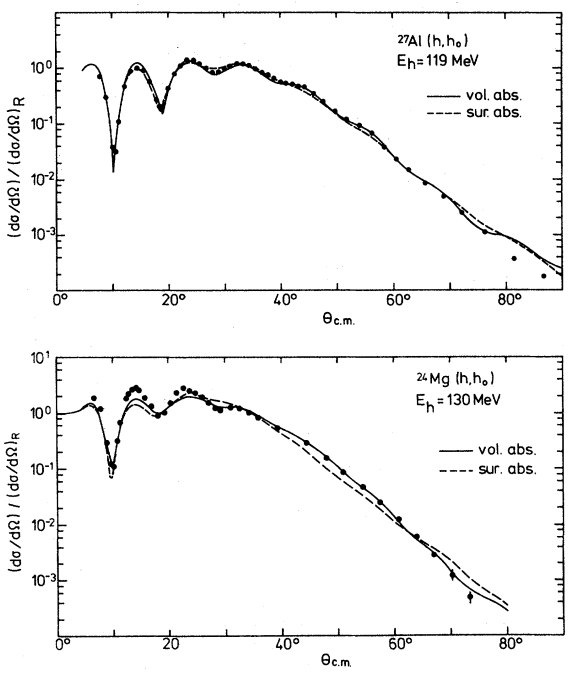

FIG. 2. Optical model fits to (a) the ^{24}Mg$(h,h_0)^{24}$Mg angular distribution at $E_h = 130$ MeV using the parameters sets DVSH and DSSH (see Table I), (b) the ^{27}Al$(h,h_0)^{27}$Al angular distribution at $E_h = 119$ MeV using the parameter sets JVSH and JSSH (see Table I).

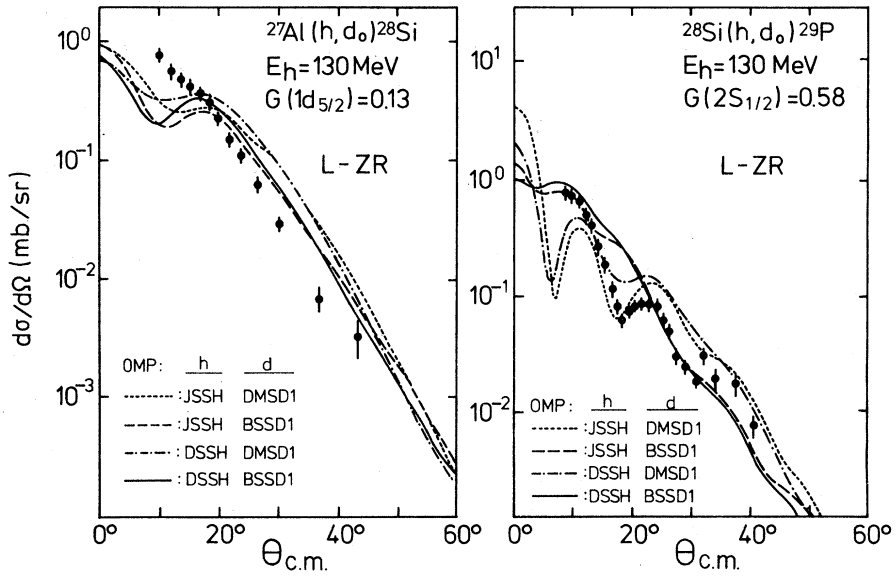

FIG. 3. Experimental angular distributions for the ^{27}Al$(h,d_0)^{28}$Si and ^{28}Si$(h,d_0)^{29}$P reactions at $E_h=130$ MeV. The curves are DWBA calculations using the parameters specified in the figure (see Table I).

nificantly larger than that found in a comprehensive analysis of Daehnick *et al.*[9] The set DMSD2 is the same as that of DMSD1 except for V_{so}, which is fixed at 6 MeV. Similarly BSSD2 differs from BSSD1 only in the value of $V_{so}=6$ MeV. In set BSSD3, $V_{so}=6$ MeV and the spin-orbit geometry is taken to be that of the real central part. The BMSD4 is extrapolated from systematics obtained recently by Bojowald *et al.*[10] The effects of using each of those deuteron optical model parameter sets (see Table I) are discussed in the next section.

In previous works,[12,13] it was found that a good DWBA description of a direct transfer reaction $(a+x)+B\rightarrow(B+x)+a$ or its inverse seems to require that the relation $V_{(a+x)}\sim V_x^b+V_a$ (see Table I) be satisfied. Here V_x^b represents the depth of the bound-state potential of the transferred particle x. In the present work the parameters of the bound-state geometry are taken to be $r_0=1.25$ fm and $a_0=0.65$ as used by other authors.[14–16] The resulting WS potential depths V_p^b were found to be 59 and 49 MeV for ^{27}Al ($1d_{5/2}$ orbit) and ^{28}Si ($2s_{1/2}$ orbit),

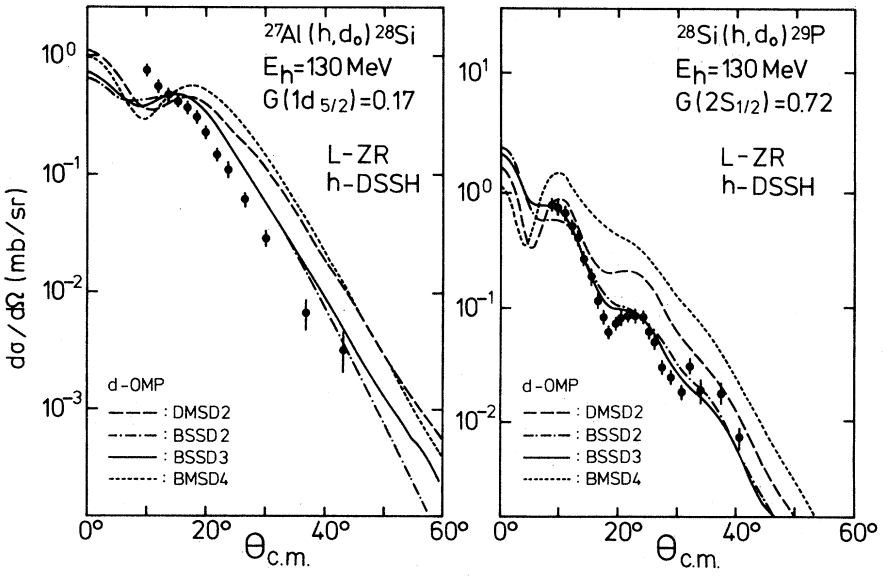

FIG. 4. See the caption to Fig. 3.

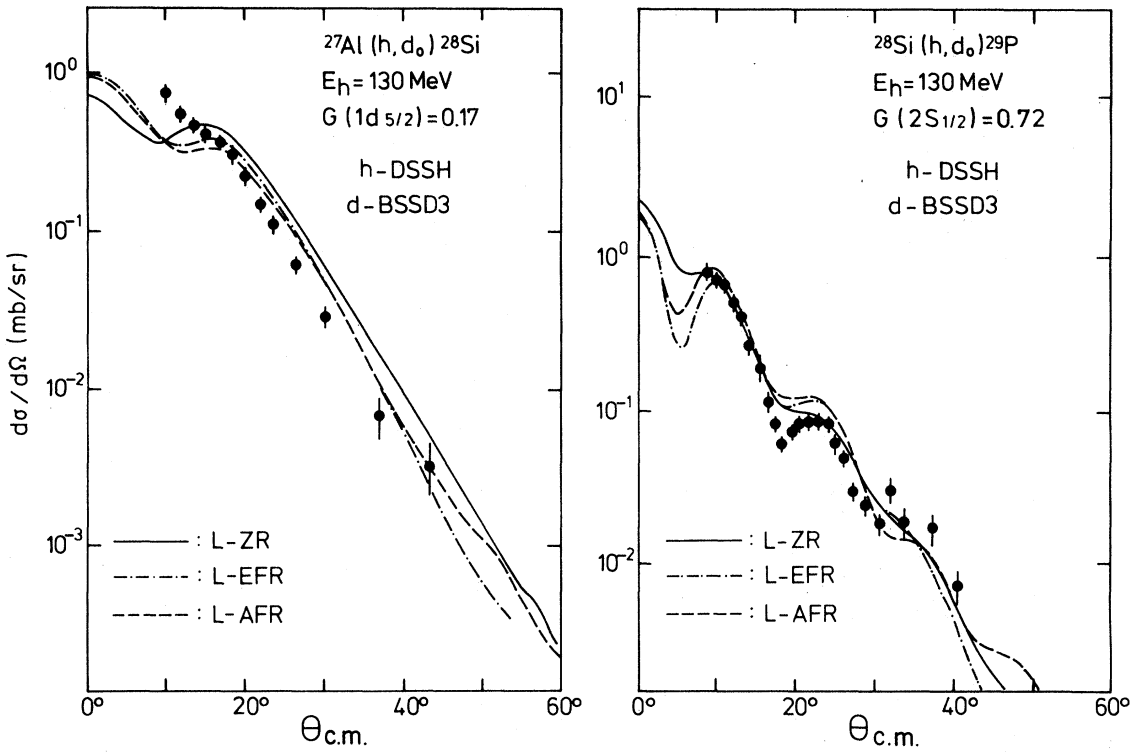

FIG. 5. See the caption to Fig. 3.

respectively. Combined with $V_d = 50$ MeV (see Table I), a helion optical potential with a depth of $V \sim 100-110$ MeV is required to satisfy the relation $V_h \sim V_d + V_p^b$. Four sets of helion optical potentials have been used in the present analysis. They have been derived as follows. The JVSH (volume absorption) and JSSH (surface absorption) sets were obtained from optical model analysis of ^{27}Al(h,h_0) data of Ref. 17 at $E_h = 119$ MeV by means of the optical model code OPTY.[18] A similar analysis was performed on ^{24}Mg(h,h_0) data measured[7] previously at $E_h = 130$ MeV to give DVSH (volume absorption) and DSSH (surface absorption) sets. The resulting fits are shown in Fig. 2.

B. Results

Figure 3 shows four sets of L-ZR (local zero-range) theoretical curves for ^{27}Al and ^{28}Si(h,d_0) reactions. These curves were calculated using two h-OMP sets (JSSH and DSSH; see Table I), each in combination with one of the two d-OMP sets (BSSD1 and DMSD1; see Table I). For a given d-OMP set, the resulting theoretical curves for the two different h-OMP sets have roughly similar shapes for both target nuclei. Similar results were obtained using JVSH and DVSH h-OMP sets (not shown in the figure). In view of this, no significant changes were expected when the "actual" h-OMP parameters extracted from ^{27}Al(h,h_0) at $E_h = 130$ MeV were used in the calculations. It can be seen that none of the curves gives a satisfactory description of the experimental data.

The predicted theoretical angular distributions calculated using the h-OMP set DSSH in combination with the other four d-OMP sets (see Table I) are shown in Fig. 4. For both ^{27}Al and ^{28}Si cases, the use of BMSD4 in the exit channel resulted in very poor fit quality. For the Daehnick extrapolation the increase of the V_{so} value from 3.0 MeV (DMSD1) to 6 MeV (DMSD2) does not result in a good fit. On the other hand, in the Bojowald case, decreasing the V_{so} value from 12.5 MeV (BSSD1) to 6 MeV (BSSD2) yields a considerable improvement; however, the overall fit quality is still poor. Similar conclusions can also be drawn for the set BSSD3 ($V_{so} = 6$ MeV and the geometry as that of the real central part). While for the ^{27}Al case both BSSD2 and BSSD3 give comparable fit quality, for the ^{28}Si case the latter potential set gives a slightly better agreement with the experimental data, in particular for $\theta_{c.m.} \leq 30°$.

Figure 5 shows the results of finite-range (FR)

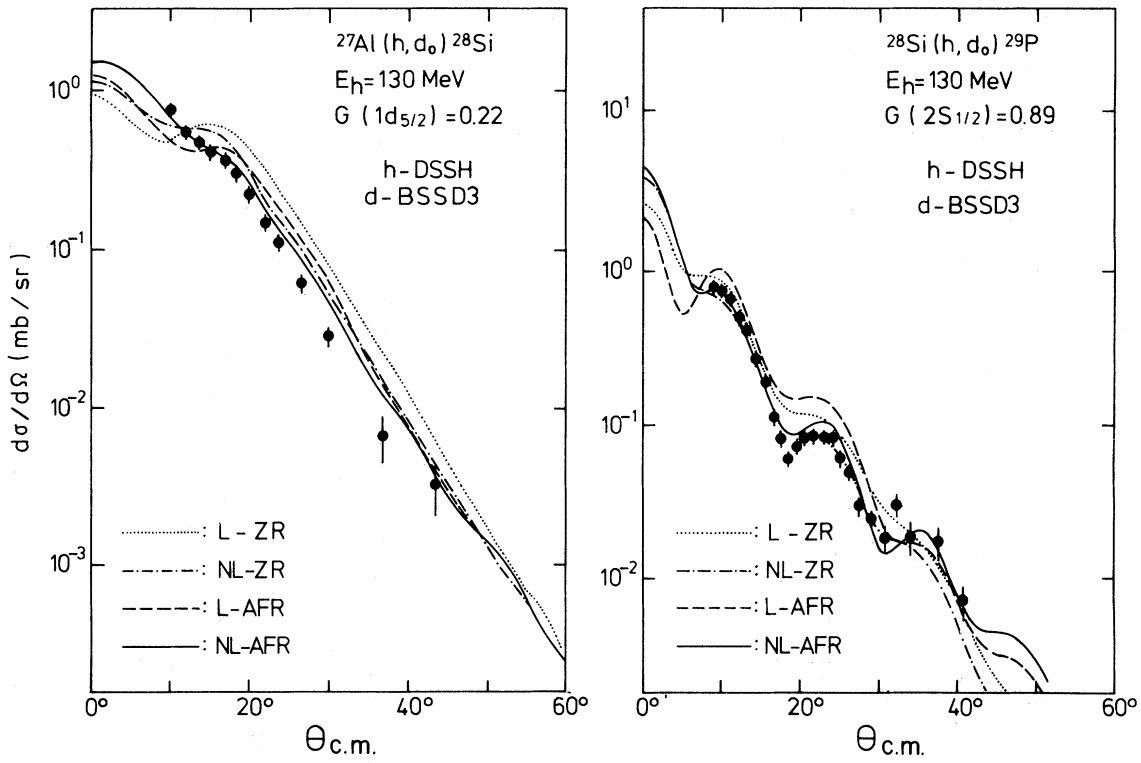

FIG. 6. See the caption to Fig. 3.

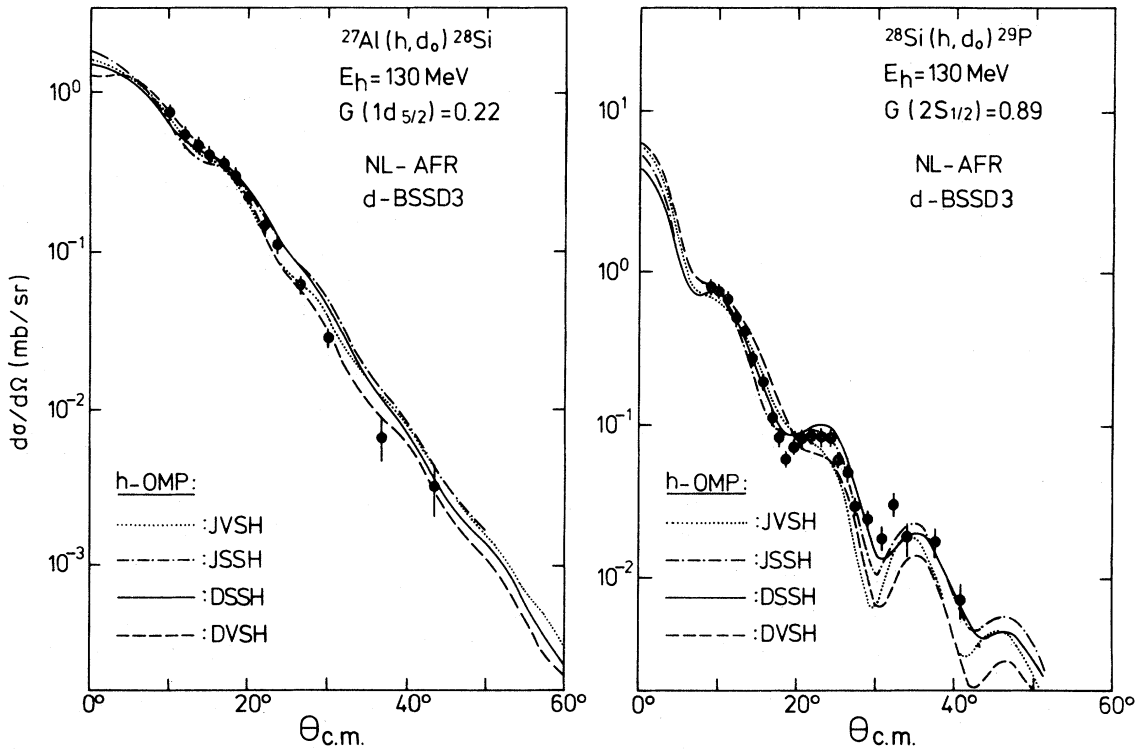

FIG. 7. See the caption to Fig. 3.

calculations performed in an exact (EFR) and an approximate (AFR) method employing the local DSSH-BSSD3 potential combination. In addition, the corresponding L-ZR curve is shown for comparison. For both ^{27}Al and ^{28}Si cases, the shapes of the L-EFR and L-AFR curves are not very dissimilar. However, the magnitude of the predicted cross sections differs up to about 30% at certain angles. In both the ^{27}Al and ^{28}Si cases, the finite range calculations still do not describe the experimental data satisfactorily. Figure 6 shows the results of including nonlocality (NL) corrections using the DWUCK4 code (see Sec. III). It can be seen that neither the NL nor FR correction alone can reproduce the experimental data. However, inclusion of both finite-range and nonlocality corrections gives a satisfactory description of the ^{27}Al and ^{28}Si (h,d_0) experimental angular distributions including also the more forward angle region of the ^{27}Al(h,d_0) data, which could not be fitted in Figs. 3—5.

For completeness, the effects of including NL and FR corrections are further investigated using all four h-OMP sets (see Table I), in combination with BSSD3. The results are presented in Fig. 7. In the ^{27}Al case, all four h-OMP sets give a satisfactory fit quality, particularly DVSH and JVSH. In the ^{28}Si case, all four h-OMP sets also describe the data reasonably well, but DSSH and JSSH have a slight preference. A similar investigation has also been made using all six d-OMP sets (see Table I) in combination with the DSSH potential set. For clarity, only the results obtained with four d-OMP sets are shown in Fig. 8. The use of the DMSD1 or DMSD2 potential set results in poor fits to both the ^{27}Al and ^{28}Si data. Similarly, poor results are also obtained for BSSD1 and BMSD4 (not shown in the figure). In the ^{27}Al case, BSSD2 and BSSD3 give comparable and satisfactory fits. On the other hand, BSSD3 gives a slightly better fit to the ^{28}Si data. In conclusion, the use of the potential set combination DSSH(h)-BSSD3(d) in the NL-AFR calculation gives the best description of the experimental data. Consequently, the DSSH-BSSD3 potential combination has been used to extract the spectroscopic strengths in the present work.

C. Spectroscopic strength

The spectroscopic strengths for the proton stripped to the ground state of the final nuclei ^{28}Si and ^{29}P extracted in this work, as well as those available in the literature, are summarized in Table II. It can be seen that for the ^{29}P case, previous ex-

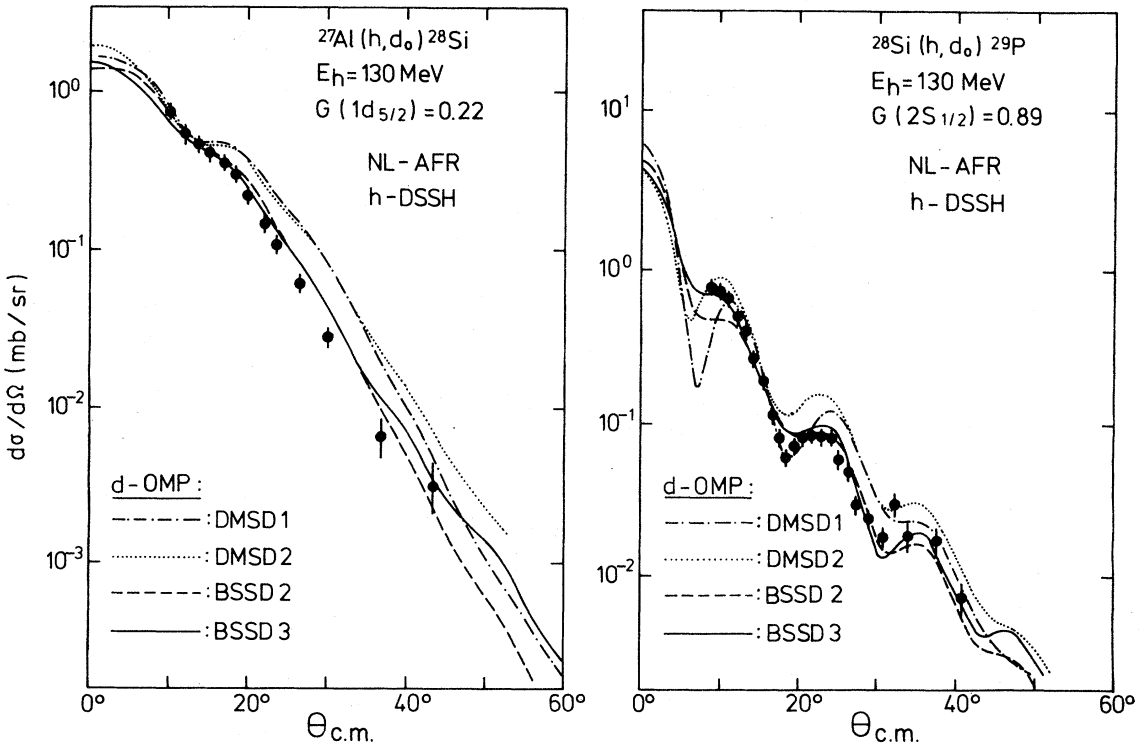

FIG. 8. See the caption to Fig. 3.

TABLE II. Spectroscopic strengths $G(nlj)=(2J_f+1)(2J_i+1)^{-1}C^2S(nlj)$ for proton stripping to the ground states of ^{28}Si and ^{29}P.

	Reaction	E_{inc} (MeV)	$G(nlj)$	Reference
	(h,d_0)	37.7	0.44	19
	(d,n_0)	6	0.25	20
	(h,d_0)	8	0.49	14
Target: ^{27}Al	(α,t_0)	104	1.0	21
$J_i^\pi=\frac{5}{2}^+$	(α,t_0)	27.2	0.44	22
$J_f^\pi=0^+$	(α,t_0)	25.2	0.58	23
$nlj=1d_{5/2}$			0.86	
			0.90	
	(h,d_0)	130	0.22±0.04	Present work
	Theory		0.53	2
			0.61	25
	(d,n_0)	7.9	1.36	26
	(h,d_0)	35.3	0.42	24
Target: ^{28}Si	(h,d_0)	38.5	1.02	15
$J_i^\pi=0^+$	(h,d_0)	25	1.30	16
$J_f^\pi=\frac{1}{2}^+$	(h,d_0)	29	1.08	27
$nlj=2s_{1/2}$	(h,d_0)	130	0.89±0.18	Present work
	Theory		1.0	2
			0.90	25

perimental $G(2s_{1/2})$ values show large discrepancies up to a factor of 3, the lowest and the highest values being 0.42 and 1.36, respectively. Similarly for ^{27}Al, experimental $G(1d_{5/2})$ values are found to vary from 0.25 to 1.0. At lower incident energies these discrepancies might reflect the inadequacy of the DWBA to describe the reaction mechanism, since at these energies indirect processes and even fluctuation in the cross sections may play a significant role. Further uncertainties are introduced because of the subjectivity in normalizing the DWBA to the experimental angular distribution, particularly when the fit is not good.

In this work the $G(2s_{1/2})$ for the ^{28}Si$(h,d_0)^{29}$P reaction is found to be 0.89±0.18. This value agrees well with that obtained (0.90) by a shell model calculation[25] performed in a full $1d_{5/2}$-$2s_{1/2}$-$1d_{3/2}$ basis space. For the ^{27}Al$(h,d_0)^{28}$Si reaction, on the other hand, the presently extracted $G(1d_{5/2})=0.22\pm0.04$ differs greatly from $G(1d_{5/2})=0.61$ predicted by the same shell model calculation.[25] The reason for this discrepancy is not understood at present, particularly, if one compares the ratio $G(2s_{1/2})/G(1d_{5/2})$ of the presently extracted spectroscopic strengths for the two transitions studied and the one predicted by the shell model. However, considering the deformation of the ^{27}Al and ^{28}Si nuclei, the neglect of the $1f$-$2p$ shell in the above shell model calculation might not be justified. How far the inclusion of the $1f$-$2p$ shell will affect the present shell model predictions remains to be seen.

IV. CONCLUSION

Results of differential cross section measurements of ^{27}Al and ^{28}Si(h,d_0) reactions at $E_h=130$ MeV incident energy are reported. The shape of the experimental angular distributions is reproduced well by the theoretical curves calculated in the framework of the single-step DWBA formalism, using $V_d\sim50$ MeV and $V_h=110$ MeV (see Sec. III A). The potential combination satisfies the relation $V_d+V_p^b\sim V_h$, where V_p^b denotes the depth of the proton bound-state potential. This finding corroborates the results obtained previously.[12,13] Inclusion of both finite-range and nonlocality corrections appears to be necessary for a good description of the present experimental data. For the ^{28}Si (h,d_0) reaction, the extracted spectroscopic strength $G(2s_{1/2})=0.89\pm0.18$ agrees well with that obtained from a shell model calculation performed in a full $1d_{5/2}$-$2s_{1/2}$-$1d_{3/2}$ basis space.[25] For the ^{27}Al(h,d_0), the value $G(1d_{5/2})=0.22\pm0.04$ is only about 40% of that theoretically predicted.[25] The reason for this discrepancy (see Sec. III C) is not understood at present. It may be, at least partly, due to deformation effects.

[1]P. M. Endt and C. van der Leun, Nucl. Phys. A310, 1 (1978).
[2]B. H. Wildenthal and J. B. McGrory, Phys. Rev. C 7, 714 (1973).
[3]A. Djaloeis *et al.* (unpublished).
[4]G. Riepe and D. Protić, IEEE Trans. Nucl. Sci. NS22, 178 (1975).
[5]P. D. Kunz, computer code DWUCK5, University of Colorado, Boulder (unpublished).
[6]P. D. Kunz, computer code DWUCK4, University of Colorado, Boulder (unpublished).
[7]A. Djaloeis, J. P. Didelez, A. Galonsky, and W. Oelert, Nucl. Phys. A306, 221 (1978).
[8]J. R. Shepard, W. R. Zimmermann, and J. J. Kraushaar, Nucl. Phys. A275, 189 (1977).
[9]W. W. Daehnick, J. D. Childs, and Z. Vrcelj, Phys. Rev. C 21, 2253 (1980), and references therein; L. D. Knutson and W. Haeberli, Phys. Rev. Lett. 30, 986 (1973); Phys. Rev. C 12, 1469 (1975).
[10]J. Bojowald, C. Mayer-Böricke, M. Rogge, and P. Turek, Institut für Kernphysik, Kernforschungsanlage Jülich Annual Report, KFA-IKP, Jül-Spez-72, 1979, p. 1, and Kernforschungsanlage Jülich Annual Report, KFA-IKP, Jül-Spez-99, 1980, p.1.
[11]P. W. Keaton and D. D. Armstrong, Phys. Rev. C 8, 1692 (1973).
[12]A. Djaloeis *et al.*, Nucl. Phys. A342, 252 (1980).
[13]R. Stock *et al.*, Nucl. Phys. A104, 136 (1967).
[14]J. Kalifa, G. Rotbard, M. Vergnes, and G. Ronsin, J. Phys. (Paris) 34, 139 (1973).
[15]R. J. Peterson and R. A. Ristinen, Nucl. Phys. A246, 402 (1975).
[16]W. W. Dykoski and D. Dehnhard, Phys. Rev. C 13, 80 (1976).
[17]M. Hyakutake *et al.*, Nucl. Phys. A333, 1 (1980).
[18]H. Dabrowski, R. Planeta, and A. Djaloeis, Institut für Kernphysik, Kernforschungsanlage Jülich report, KFA-IKP Jül-Report-1637, (1979).
[19]R. W. Barnard and G. D. Jones, Nucl. Phys. A108, 641 (1968).
[20]W. Bohne *et al.*, Nucl. Phys. A131, 273 (1969).
[21]G. Hauser *et al.*, Nucl. Phys. A182, 1 (1972).
[22]O. F. Nemets *et al.*, Ukr. Fiz. Zh. (Russ. Ed.) 22, 246 (1977).
[23]V. M. Lebedev *et al.*, Nucl. Phys. A298, 206 (1978).
[24]P. Leleux, P. C. Macq, J. P. Meulders, and C. Pirart, Z. Phys. 271, 139 (1974).
[25]W. Chung and B. H. Wildenthal (private communication).
[26]Buccino *et al.*, Nucl. Phys. 86, 353 (1966).
[27]Koyama *et al.*, J. Phys. Soc. Jpn. 43, 755 (1977).